Model Predictive Flux Control With Cost Function-Based Field Weakening Strategy for Permanent Magnet Synchronous Motor

Zhihao Zheng and Dan Sun, *Senior Member, IEEE*

***Abstract*—This paper proposes a model predictive flux control (MPFC) strategy with cost function-based field weakening (FW) strategy for permanent magnet synchronous motor (PMSM). The stator flux vector is used as the control variable and the cost function of the proposed MPFC is configured in the form of flux increment, which can reflect the saturation degree of the inverter output. A novel space flux vector plane is introduced to explain the principle of optimal switching state selection in the proposed MPFC. The voltage and current limitations of the inverter in the high-speed region are analyzed in the flux plane to reveal the objective of FW compensation. The value of the cost function is controlled with a proportional integral controller in the proposed cost function-based FW strategy. Moreover, the reference flux vector is compensated with the output of the FW controller to enlarge the operation region of the stator flux vector. With the proposed FW strategy, the operation range of the PMSM is extended and the torque output in high-speed range is increased. Experimental studies are carried out to verify the validity and effectiveness of the proposed strategy.**

***Index Terms*—Field weakening (FW) control, model predictive flux control (MPFC), permanent magnet synchronous motor (PMSM).**

NOMENCLATURE

ref	Reference value.
u_d, u_q	*d–q* components of stator voltage.
i_d, i_q	*d–q* components of stator current.
ψ_d, ψ_q	*d–q* components of stator flux linkage.
L_d, L_q	*d–q* components of stator inductance.
R_s	Stator winding resistance.
ω_e	Rotor electrical angular speed.
$\psi_{\rm f}$	Permanent magnet flux linkage.
T_e	Electromagnetic torque.
n_p	Number of pole pairs.
T_s	Sampling period.
θ_r	Rotor angle.
p	Differential operator.
$V_{\rm dc}$	DC-link voltage.

Manuscript received December 24, 2018; revised April 13, 2019; accepted June 1, 2019. Date of publication June 5, 2019; date of current version November 12, 2019. This work was supported by the National Natural Science Foundation of China under Grant 51877197. Recommended for publication by Associate Editor M. Su. *(Corresponding author: Dan Sun.)*

The authors are with the College of Electrical Engineering, Zhejiang University, Hangzhou 310027, China (e-mail: zzh9322@126.com; sundan@zju.edu.cn).

Color versions of one or more of the figures in this paper are available online at http://ieeexplore.ieee.org.

Digital Object Identifier 10.1109/TPEL.2019.2921361

I. INTRODUCTION

PERMANENT magnet synchronous motors (PMSMs) have attractive advantages including high efficiency, excellent control performance, and high power density [1]. In order to realize high-performance control of PMSM, more demands are required for the modern control strategies, including fast dynamic response, adaptive for multiple control constraints and wide operation range.

Field-oriented control (FOC) and direct torque control (DTC) are two classical control strategies applied in industrial applications [2]–[5]. In FOC, proportional integral (PI) controllers are used to control the decomposed stator currents in synchronous rotatory frame [2], [3]. The space vector modulation is used to generate the pulses with constant switching frequency. The torque and flux in FOC can be controlled precisely but the parameters of the controllers require fine tuning work. In DTC, two hysteresis comparators are used to select the voltage vector with a predefined switching table [4], [5]. The DTC has fast dynamic response and good robustness against parameter changes, but it also features drawbacks of high torque ripples and variable switching frequency.

Model predictive control (MPC) is also considered as an effective control strategy with fast dynamic response and manageable constraints [6]–[16]. The development of microprocessors with powerful computational ability makes it possible for the implementation of MPC in electrical drives. In MPC, the discretized mathematical model of PMSM is established to predict the current, flux, or torque behaviors in the future control periods. A cost function that contains the errors of the control variables is used to select the optimal output of the controller. Different control objectives can be easily incorporated in the constraints of the cost function [7], [13]–[16].

Model predictive torque control (MPTC) is a typical torque control strategy implemented with MPC [7]–[9]. In MPTC, the torque and stator flux are simultaneously evaluated in the cost function to realize optimal control of both torque and stator flux. However, the control variables contained in the cost function of MPTC have different units and magnitudes. The weighting factors of different constraints need to be well tuned, otherwise, the performance of the PMSM system will deteriorate. Model predictive flux control (MPFC) is an alternative MPC strategy to avoid the tuning work of the weighting factors in MPTC [10]–[12]. The reference torque and amplitude of the stator flux

are converted into an equivalent reference flux vector. Therefore, the constraints in the cost function have same units and magnitudes and the weighting factors are eliminated. In the previous research works of MPFC, the optimization of switching instant [11] and simplified voltage selection [12] are studied. However, the limitation and operation trajectory of the stator flux vector in different operation range has not been analyzed thoroughly. Especially in the high-speed range, the operation range of the PMSM system is restricted by the voltage and current limitations of the inverter. In this case, field weakening (FW) strategy is required to compensate the stator flux vector and improve the performance of the PMSM system in high-speed range.

Incorporation of FW strategy into MPC strategies is an essential concern for PMSM operating at high speed. To realize FW operation in MPTC strategies, the reference torque and flux magnitude are simply set to be proportional to the inverse of the rotor speed in [13]. Despite the simplicity of this method, it only considers the voltage limitation but the variation of stator current is neglected. For current-based MPC algorithms, the voltage control loop is used to compensate the reference current for high-speed operation [14]. This FW algorithm is robust against motor parameters variation but the effectiveness is easily disturbed by the variation of the dc-link voltage. The work in [15] adds incremental voltage as another constraint of the cost function to suppress the influence of undesired disturbance from dc-link voltage, but the new cost function is more complicated and the tuning work of weighting factor is required. In [16], the torque and stator flux references are adjusted online to improve the torque capability during FW operation, but the restrictions of the switching losses and neutral point voltage error also introduce more weighting factors in the cost function.

In this paper, an MPFC with simple cost function-based FW strategy is proposed to expand the operation range of the PMSM system without introducing additional FW constraints in the cost function. The flux increment is used as the control variable in the cost function of the proposed MPFC, which reflects the saturation degree of the inverter. The value of the cost function is controlled in an acceptable range to keep the PMSM system operating within the voltage and current limits in the FW region. The limitation and operation trajectory of the stator flux vector are analyzed to support the proposed FW strategy.

The rest of this paper is organized as follows: The mathematical models of PMSM and the discrete-time model are introduced in Section II. The principle of the proposed MPFC strategy is analyzed in Section III. The principle of the proposed cost function-based FW strategy in MPFC is introduced in Section IV. Experimental results are given in Section V to validate the effectiveness of the proposed control strategy. The conclusion is presented in the last section.

II. Mathematical Model of PMSM

The dynamic models of PMSM in the *d–q* synchronous rotatory frame can be described as following equations:

The stator voltage of PMSM can be obtained as follows:

$$\begin{bmatrix} u_d \\ u_q \end{bmatrix} = R_s \begin{bmatrix} i_d \\ i_q \end{bmatrix} + \begin{bmatrix} p & -\omega_e \\ \omega_e & p \end{bmatrix} \begin{bmatrix} \psi_d \\ \psi_q \end{bmatrix}. \tag{1}$$

The stator flux linkage of PMSM can be obtained as follows:

$$\begin{bmatrix} \psi_d \\ \psi_q \end{bmatrix} = \begin{bmatrix} L_d & 0 \\ 0 & L_q \end{bmatrix} \begin{bmatrix} i_d \\ i_q \end{bmatrix} + \begin{bmatrix} \psi_f \\ 0 \end{bmatrix}. \tag{2}$$

The electromagnetic torque can be obtained as follows:

$$T_e = \frac{3}{2} n_p \boldsymbol{\psi}_s \otimes \boldsymbol{i}_s = \frac{3}{2} n_p (\psi_d i_q - \psi_q i_d) \tag{3}$$

where $\boldsymbol{\psi}_s$ is the stator flux vector and $\boldsymbol{i}_s$ is the stator current vector.

In digital processing implementation, the dynamic mathematical model can be discretized to predict the states of variables in the future. The discrete-time model can be obtained by the Euler method without introducing additional unwanted nonlinear terms [17]. According to (1), the stator flux linkage in k+1 instant can be predicted as follows:

$$\begin{bmatrix} \psi_d(k+1) \\ \psi_d(k+1) \end{bmatrix} = \begin{bmatrix} 1 & \omega_e T_s \\ -\omega_e T_s & 1 \end{bmatrix} \begin{bmatrix} \psi_d(k) \\ \psi_q(k) \end{bmatrix} - R_s T_s \begin{bmatrix} i_d(k) \\ i_q(k) \end{bmatrix} + T_s \begin{bmatrix} u_d(k) \\ u_q(k) \end{bmatrix}. \tag{4}$$

III. Principle of the Proposed MPFC

A. Reference Stator Flux Vector

The electromagnetic torque equation in (3) shows that T_e is decided by the stator flux vector $\boldsymbol{\psi}_s$ and the current vector $\boldsymbol{i}_s$. The relationship between T_e and $\boldsymbol{\psi}_s$ can be established according to a certain current control method. Maximum torque per ampere control and $i_d = 0$ control methods are two well-known current control methods [18], [19]. In this paper, the $i_d = 0$ control method is applied in the proposed MPFC strategy due to its concise form to reveal the control principle. The reference stator flux vector in the proposed MPFC can be converted from the reference torque according to the $i_d = 0$ control method.

Based on the $i_d = 0$ control method, the electromagnetic torque in (3) can be expressed as follows:

$$T_e = \frac{3}{2} n_p \psi_d i_q. \tag{5}$$

When the reference torque $T_{\mathrm{e}}^{\mathrm{ref}}$ is given, the *d–q* components of the reference stator flux vector $\boldsymbol{\psi}_s^{\mathrm{ref}}$ can be obtained as follows:

$$\begin{aligned} \psi_d^{\mathrm{ref}} &= \psi_f \\ \psi_q^{\mathrm{ref}} &= 2L_{\mathrm{q}} T_{\mathrm{e}}^{\mathrm{ref}} / 3 n_p \psi_f. \end{aligned} \tag{6}$$

It can be seen from (6) that the control of torque can be realized by tracking the reference stator flux vector $\boldsymbol{\psi}_s^{\mathrm{ref}}$.

B. Prediction Model of Stator Flux

The prediction model of $\boldsymbol{\psi}_s(k+1)$ in (4) contains different kinds of variables, including stator flux, voltage, and current. In order to simplify the explanation of the proposed MPFC strategy, the prediction model of stator flux is reconfigured with flux variables.

The prediction model of $\boldsymbol{\psi}_s(k+1)$ in (4) can be rewritten as follows:

$$\boldsymbol{\psi}_s(k+1) = \boldsymbol{\psi}_0(k) + \Delta\boldsymbol{\psi}_s(k) \tag{7}$$

where $\psi_0(k)$ is the initial flux linkage and $\Delta\boldsymbol{\psi}_s(k)$ is the flux increment.

The initial flux linkage $\psi_0(k)$ represents the state of flux linkage in k instant, which can be estimated with the observers. The initial flux linkage $\psi_0(k)$ is defined as follows:

$$\begin{bmatrix}\psi_{0d}(k)\\ \psi_{0q}(k)\end{bmatrix} = \begin{bmatrix}1 & \omega_e T_s\\ -\omega_e T_s & 1\end{bmatrix}\begin{bmatrix}\psi_d(k)\\ \psi_q(k)\end{bmatrix} - R_s T_s \begin{bmatrix}i_d(k)\\ i_q(k)\end{bmatrix}. \tag{8}$$

The flux increment $\Delta\boldsymbol{\psi}_s(k)$ represents the flux increment produced by the inverter in k instant. Assuming that the stator voltage applied in the entire sampling period T_s, the flux increment $\Delta\boldsymbol{\psi}_s(k)$ can be obtained as follows:

$$\Delta\boldsymbol{\psi}_s(k) = \boldsymbol{u}_s(k)\,T_s \tag{9}$$

where $\boldsymbol{u}_s(k)$ is the stator voltage vector in k instant.

In the signal processing implementation, the controller works one sampling period after the observer and the voltage applied to the stator winding takes effect on the stator flux after one more control period [20]. Considering the one-step delay effect during the sampling and control process, the stator flux in k+2 instant is predicted and the prediction model in (7) should be rewritten as follows:

$$\boldsymbol{\psi}_s(k+2) = \boldsymbol{\psi}_0(k) + \Delta\boldsymbol{\psi}_s(k+1). \tag{10}$$

C. Evaluation of Cost Function

The cost function in MPFC is usually defined as the tracking error of the stator flux [12], which can be expressed as follows:

$$\begin{aligned} C &= \left|\psi_d{}^{\mathrm{ref}} - \psi_d(k+2)\right|^2 + \left|\psi_q{}^{\mathrm{ref}} - \psi_q(k+2)\right|^2 \\ &= \left|\boldsymbol{\psi}_s{}^{\mathrm{ref}} - \boldsymbol{\psi}_s(k+2)\right|^2. \end{aligned} \tag{11}$$

Substituting (10) into (11), the cost function C can be written as follows:

$$C = \left|\boldsymbol{\psi}_s{}^{\mathrm{ref}} - \boldsymbol{\psi}_0(k) - \Delta\boldsymbol{\psi}_s(k+1)\right|^2. \tag{12}$$

The reference flux increment $\Delta\boldsymbol{\psi}_s^{\mathrm{ref}}$ is defined as the difference between $\boldsymbol{\psi}_s^{\mathrm{ref}}$ and $\psi_0(k)$, which represents the flux increment required for the initial flux linkage to follow the reference stator flux vector. The reference flux increment $\Delta\boldsymbol{\psi}_s^{\mathrm{ref}}$ can be written as follows:

$$\Delta\boldsymbol{\psi}_s{}^{\mathrm{ref}} = \boldsymbol{\psi}_s{}^{\mathrm{ref}} - \boldsymbol{\psi}_0(k). \tag{13}$$

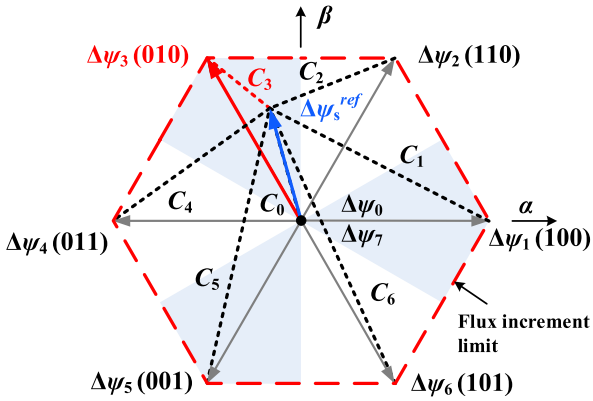

Fig. 1. Basic flux vectors in the space flux plane.

Substituting (13) into (12), the cost function C can be written as follows:

$$C = \left|\Delta\boldsymbol{\psi}_s{}^{\mathrm{ref}} - \Delta\boldsymbol{\psi}_s(k+1)\right|^2. \tag{14}$$

In order to minimize the tracking error of the stator flux vector, the flux increment $\Delta\boldsymbol{\psi}_s(k+1)$ applied in k+1 instant should be selected to minimize the cost function. The value of the cost function in (14) also reflects the output ability of the inverter. When the maximum output of the inverter cannot satisfy the requirement of the reference flux increment, the value of the cost function in (14) becomes large, so as the tracking error of the stator flux vector.

D. Optimal Selection of Flux Increment

The switching states of the three-phase voltage source inverter can be denoted as binary variables S_a, S_b, and S_c. The switching state of each phase equals to "1" when the upper switch is ON and the bottom switch is OFF and "0" for the reverse ON–OFF state. There are eight switching states of the three-phase inverter, denoted as S_n (000, 100, 110, 010, 011, 001, 101, and 111). The flux increment $\Delta\boldsymbol{\psi}_s$ can be calculated according to the switching states as follows:

$$\begin{bmatrix}\Delta\psi_{sd}\\ \Delta\psi_{sq}\end{bmatrix} = \begin{bmatrix}u_d\\ u_q\end{bmatrix}\cdot T_s = \frac{2}{3}V_{\mathrm{dc}}T_s\cdot\boldsymbol{M}\cdot\begin{bmatrix}S_a\\ S_b\\ S_c\end{bmatrix} \tag{15}$$

where

$$\boldsymbol{M} = \begin{bmatrix}\cos\theta_r & \cos(\theta_r - \frac{2\pi}{3}) & \cos(\theta_r + \frac{2\pi}{3})\\ -\sin\theta_r & -\sin(\theta_r - \frac{2\pi}{3}) & -\sin(\theta_r + \frac{2\pi}{3})\end{bmatrix}.$$

A novel space flux vector plane is established to describe the relationship between the switching state S_n and the flux increment $\Delta\psi_s$. Each switching state S_n corresponds to a basic flux vector $\Delta\boldsymbol{\psi}_n(n = 0, 1\ldots 7)$. The basic flux vector $\Delta\boldsymbol{\psi}_n$ represents the flux increment produced by the inverter when the corresponding switching state operates in an entire sampling period T_s. The basic flux vectors in the space flux vector plane in the α–β stationary frame are shown in Fig. 1.

The principle of optimal flux increment selection can be explained in the space flux vector plane. With the given reference flux increment $\Delta\boldsymbol{\psi}_s^{\mathrm{ref}}$, the value of cost function can be evaluated by substituting $\Delta\boldsymbol{\psi}_n$ into (14). As shown in Fig. 1, C_n $(n = 0, 1 \ldots 7)$ represents the distance between $\Delta\boldsymbol{\psi}_s^{\mathrm{ref}}$ and $\Delta\boldsymbol{\psi}_n$ and reflects the value of the cost function. In Fig. 1, $\Delta\psi_3$ (010) is the closest basic flux vector to $\Delta\boldsymbol{\psi}_s^{\mathrm{ref}}$ and the optimal flux vector that minimizes the cost function. Therefore, C_3 is the optimal value of cost function C_{opt} and S_3 (010) is selected as the optimal switching state that operates in k+1 instant. With the space flux vector plane, the selection of optimal switching state and the value of cost function are more intuitive to understand.

The maximum available flux increment produced by the inverter can be described with a flux increment limit hexagon that connects the terminal vertex of the basic flux vectors $\Delta\boldsymbol{\psi}_n(n = 1, 2 \ldots 6)$, as shown in Fig. 1. When the reference flux increment $\Delta\boldsymbol{\psi}_s^{\mathrm{ref}}$ locates within the flux increment limit hexagon, the maximum tracking error of the stator flux vector can be calculated as follows:

$$C_{\mathrm{opt}} = \left|\Delta\boldsymbol{\psi}_s{}^{\mathrm{ref}} - \Delta\boldsymbol{\psi}_s\,(k+1)\right|^2 \le \left|\Delta\psi_n\right|^2 = \left|\frac{2}{3}V_{\mathrm{dc}} \cdot T_s\right|^2. \tag{16}$$

Although the tracking error of the stator flux vector in the proposed MPFC strategy cannot be eliminated, it is essential to maintain the tracking error in an acceptable range. Otherwise, the tracking error of the stator flux is large and the steady-state performance of the PMSM system will deteriorate.

IV. Cost Function-Based Field Weakening Strategy

When the PMSM operates in the FW region, the output of the inverter is restricted by the voltage and current limitations and the operation range is limited. In this section, the voltage and current limitations of the inverter are transformed as the limitation of the stator flux vector. The operation trajectory of the stator flux is analyzed in ψ_d–ψ_q plane to explain the FW control objective. In order to realize FW operation, a novel cost function-based FW strategy is proposed. The value of cost function is controlled with a PI controller and the output of the controller is used to compensate the reference stator flux vector in the FW region. The operation region of the stator flux vector is extended with the proposed FW strategy.

A. Voltage and Current Limitations

The operation of PMSM in the high-speed range is limited by the capacity of the inverter. The main restrictions of the inverter are voltage and current limits. The restriction functions of stator voltage and current are given as follows:

$$u_d^2 + u_q^2 \le U_{\max}^2 \tag{17}$$

$$i_d^2 + i_q^2 \le I_{\max}^2 \tag{18}$$

where $U_{\max}$ is the voltage limit and $I_{\max}$ is the current limit.

In the steady state, by neglecting the voltage drop on the stator winding resistance, the stator voltage function in (1) can be rewritten as follows:

$$\begin{bmatrix} u_d \\ u_q \end{bmatrix} = \begin{bmatrix} 0 & -\omega_e \\ \omega_e & 0 \end{bmatrix} \begin{bmatrix} \psi_d \\ \psi_q \end{bmatrix}. \tag{19}$$

Substituting (19) into (17), the voltage restriction function can be written with the flux variables as follows:

$$\psi_d{}^2 + \psi_q{}^2 \le \left(\frac{U_{\max}}{\omega_e}\right)^2. \tag{20}$$

Substituting (2) into (18), the current restriction function can be written with the flux variables as follows:

$$\left(\frac{\psi_d - \psi_f}{L_d}\right)^2 + \left(\frac{\psi_q}{L_q}\right)^2 \le I_{\max}{}^2. \tag{21}$$

According to the voltage and current restriction functions in (20) and (21), the voltage and current limit curves can be drawn in the ψ_d–ψ_q plane. Hence, the voltage and current limitations of the inverter are transformed as the limitation of the stator flux vector. It can be seen in Fig. 2 that the voltage limit curve is a circle with the center on O(0, 0) and radius of $U_{\max}/\omega_e$. The radius of the voltage limit circle decreases as the rotor speed increases. The current limit curve is an ellipse with the center on $\mathrm{O}_1(\psi_f, 0)$. The constant electromagnetic torque curves (T_{em1}, T_{em2}, and T_{em3}) are also shown in Fig. 2. When the PMSM operates with $i_d = 0$ control method, the operation trajectory of the stator flux vector moves along AO_1 with different load conditions.

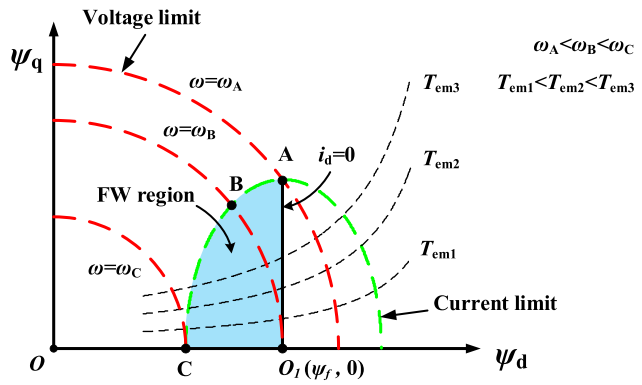

Fig. 2. Inverter limits and operation trajectory of stator flux vector in the ψ_d–ψ_q plane.

In the low speed range, the stator flux operates on the trajectory of $i_d = 0$ control method (i.e., AO_1). As the rotor speed increases, the radius of the voltage limit circle decreases continuously. When the voltage limit circle intersects the current limit ellipse and AO_1 at point A, the PMSM enters the high-speed region.

If the PMSM operates without FW strategy, the operation trajectory of the stator flux goes from point A to point O_1 with the increased speed. The maximum torque output deceases rapidly as the speed increases. The maximum speed will be ω_B when the voltage limit circle intersects AO_1 at point O_1.

When the PMSM operates at high speed, the operation trajectory of the stator flux should be extended to the FW region,

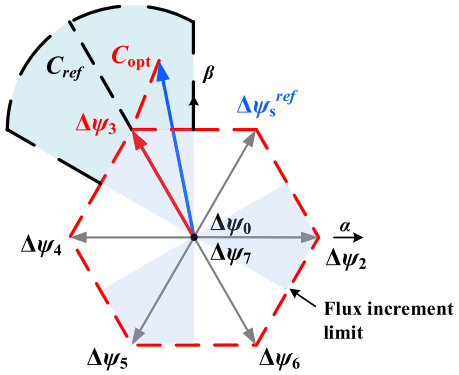

Fig. 3. Diagram of the flux vectors in the FW region.

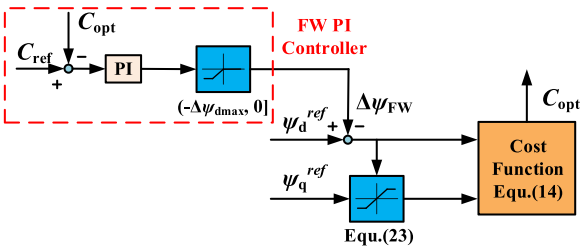

Fig. 4. Diagram of the cost function-based FW control module.

which has the voltage and current limits as its boundary. When the operation point exceeds the boundary of the FW region, the reference flux vector should be compensated with FW strategy to keep the stator flux vector within the limitation. In the FW region, the maximum speed will be extended to ω_C when the voltage limit circle intersects the current limit ellipse at point C.

Fig. 2 presents the flux compensation objective in the high-speed range. By modifying the reference flux vector to FW region, the operation trajectory of the stator flux vector is maintained within the inverter limits and therefore, the inverter is capable to produce the reference flux increment.

B. Cost Function-Based FW Strategy

In order to compensate the reference flux vector in the FW region, a cost function-based FW strategy is proposed. In the FW region, when the reference flux vector $\boldsymbol{\psi}_s^{\mathrm{ref}}$ locates outside the voltage limit circle, the inverter is unable to produce the required flux increment to track on the reference value. In this case, the terminal vertex of the reference flux increment $\Delta\boldsymbol{\psi}_s^{\mathrm{ref}}$ goes beyond the flux increment limit hexagon. The schematic diagram of the flux vectors in FW region is shown in Fig. 3.

In order to reduce the amplitude of $\Delta\boldsymbol{\psi}_s^{\mathrm{ref}}$, the reference flux vector $\boldsymbol{\psi}_s^{\mathrm{ref}}$ needs to be compensated in the FW region. When the optimal value of the cost function C_{opt} is larger than the reference value C_{ref}, the reference flux vector $\boldsymbol{\psi}_s^{\mathrm{ref}}$ is compensated with the output of the FW PI controller $\Delta\psi_{\mathrm{FW}}$. In this way, the reference flux vector $\boldsymbol{\psi}_s^{\mathrm{ref}}$ is kept within the voltage and current limits to realize FW operation.

The block diagram of the cost function-based FW control module is shown in Fig. 4. The inputs of the PI controller are the optimal value of the cost function C_{opt} and the reference value of the cost function C_{ref}. C_{ref} is set as the maximum tracking error in the constant torque region to ensure that the output of the PI controller is zero when $\Delta\boldsymbol{\psi}_s^{\mathrm{ref}}$ locates within the flux increment hexagon. The optimal value of cost function C_{opt} is controlled to follow the reference value of cost function C_{ref} and meets the following equation:

$$C_{\mathrm{opt}} = \left|\Delta\boldsymbol{\psi}_s{}^{\mathrm{ref}} - \Delta\boldsymbol{\psi}_s\,(k+1)\right|^2 \le C_{\mathrm{ref}} = \left|\frac{2}{3}V_{\mathrm{dc}}\cdot T_s\right|^2. \tag{22}$$

The output of the PI controller $\Delta\psi_{\mathrm{FW}}$ is used to compensate the reference stator flux vector $\boldsymbol{\psi}_s^{\mathrm{ref}}$ and keep the operation trajectory of the stator flux vector within the voltage and current limits. The reference stator flux vector $\boldsymbol{\psi}_s^{\mathrm{ref}}$ in (6) can be compensated with the FW component $\Delta\psi_{\mathrm{FW}}$ as follows:

$$\begin{aligned}\psi_d^{\mathrm{ref}} &= \psi_f + \Delta\psi_{\mathrm{FW}}\\ \psi_q^{\mathrm{ref}} &\le L_q\cdot\sqrt{{I_{\max}}^2 - \left(\frac{\psi_d^{\mathrm{ref}}-\psi_f}{L_d}\right)^2}.\end{aligned} \tag{23}$$

In (23), ψ_d^{ref} is compensated with $\Delta\psi_{\mathrm{FW}}$ and ψ_q^{ref} is limited according to (21) to maintain the reference flux vector $\boldsymbol{\psi}_s^{\mathrm{ref}}$ within the current limit. $\Delta\psi_{\mathrm{FW}}$ is limited in the range of $(-\Delta\psi_{d\max}, 0]$, where $\Delta\psi_{d\max}$ is the maximum compensated d-axis flux. The value of $\Delta\psi_{d\max}$ is the length of CO_1 in Fig. 2 and it can be calculated according to (21) as follows:

$$\Delta\psi_{d\max} = L_d\cdot I_{\max}. \tag{24}$$

When the reference stator flux vector is kept within the voltage and current limits, the inverter is able to produce the required flux increment during the control period. Therefore, the proposed cost function-based FW strategy can realize FW operation of the PMSM system at high speed. It can be seen from (16) and (22) that the maximum tracking errors of the flux increment are controlled within a finite error and therefore the stability of the proposed method is guaranteed in both constant torque and FW region [21].

C. Control Block Diagram

The control block diagram of the proposed MPFC with cost function-based FW strategy for PMSM system is shown in Fig. 5. The stator current i_{abc} and rotor angle θ_{r} are obtained with the current sampling module and rotor position observer. The d–q components of the reference flux vector ψ_d^{ref} and ψ_q^{ref} are calculated according to $i_d = 0$ control method with the reference torque T_e^{ref}. The initial flux vector ψ_0 is estimated with the rotor electrical angular speed ω_e, rotor angle θ_{r}, and the stator current i_{abc}. The reference flux increment $\Delta\boldsymbol{\psi}_s^{\mathrm{ref}}$ is calculated with the reference flux vector $\boldsymbol{\psi}_s^{\mathrm{ref}}$ and initial flux ψ_0. By substituting $\Delta\boldsymbol{\psi}_s^{\mathrm{ref}}$ and different basic flux vectors $\Delta\boldsymbol{\psi}_n$ into the cost function, the optimal value of cost function C_{opt} is gained.

The cost function-based FW strategy is realized with a FW PI controller. The optimal and reference value of the cost function, C_{opt} and C_{ref}, are inputs of the FW PI controller.

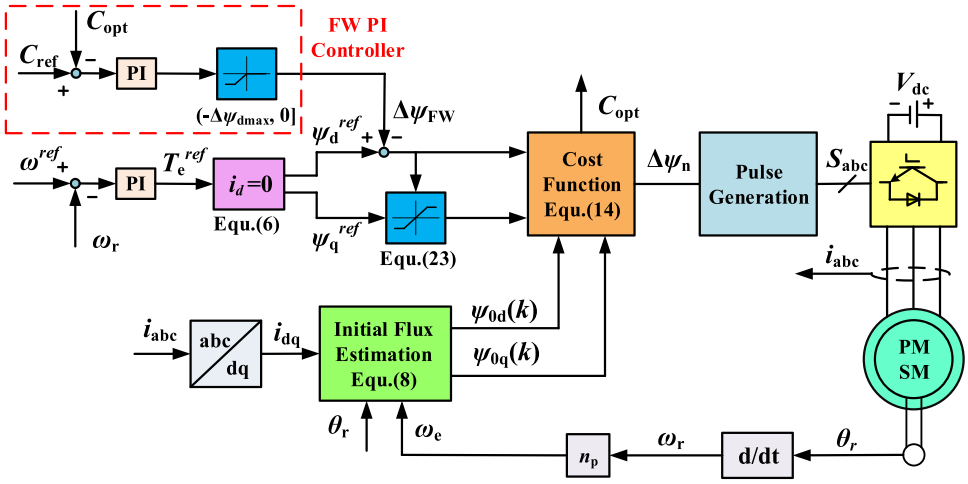

Fig. 5. Control block diagram of the proposed MPFC with cost function-based FW strategy.

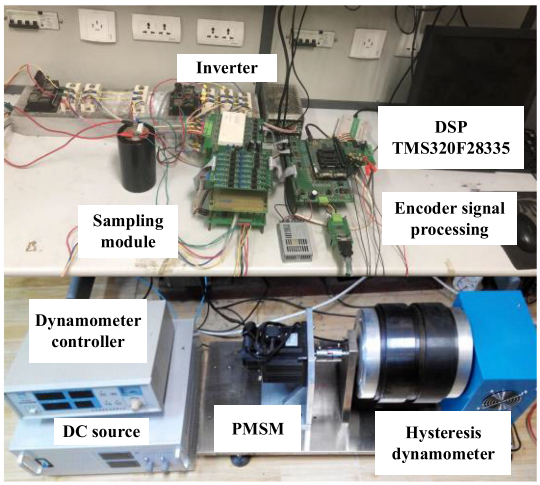

Fig. 6. Experimental equipment of the PMSM system.

TABLE I
PARAMETERS OF THE PMSM SYSTEM

Symbol	System Parameters	Value
R_s	Stator resistance	1.35 Ω
L_d	Direct inductance	5.86 mH
L_q	Quadrature inductance	11.05 mH
V_{dc}	DC-link voltage	90 V
n_p	Number of pole-pairs	4
ψ_f	Permanent magnet flux linkage	0.1547 Wb
T_s	Sampling period.	0.0001 s
U_{max}	Maximum stator voltage	52 V
I_{max}	Maximum stator current	7.07 A

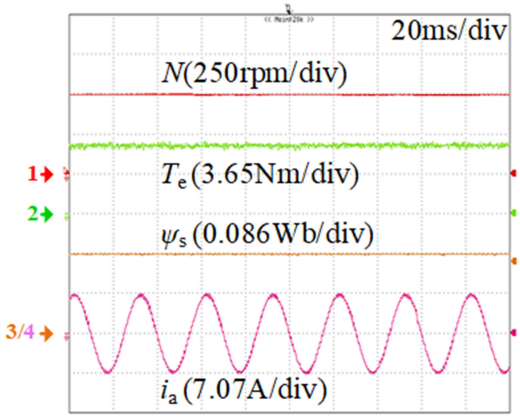

Fig. 7. Steady-state performance of the PMSM with maximum achievable torque output at 500 r/min.

The output of the FW PI controller $\Delta\psi_{\rm FW}$ is used to compensate the d-axis component of the reference flux vector $\psi_d^{\rm ref}$ and the q-axis component of the reference flux vector $\psi_q^{\rm ref}$ is limited according to the current limit function. Finally, the pulse signals for the switching states S_{abc} are generated to drive the three-phase inverter.

V. EXPERIMENTAL STUDIES

The effectiveness of the proposed MPFC with cost function-based FW strategy is verified with experimental studies. The steady-state performances of the MPFC strategy at both low and high speeds are investigated. The comparison of the MPFC with and without FW strategy is given to verify the enhancement of the proposed FW strategy in the high-speed region. For safety concern, the dc-link voltage is decreased to 90 V to limit the maximum speed of the PMSM.

The experimental equipment is shown in Fig. 6. The inverter is built with SEMIKRON SKM75GB12T4 IGBTs and driven by SEMIKRON SKHI61. The experimental studies are carried out based on TI DSP TMS320F28335 controller board. Parameters of the PMSM system are listed in Table I. The experimental results are shown in Figs. 7–12.

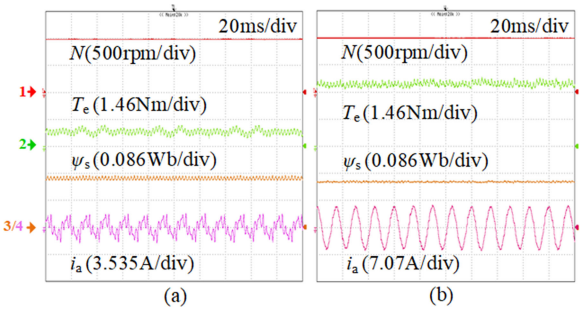

Fig. 8. Steady-state performance of the PMSM with maximum achievable torque output at 1000 r/min. (a) Without FW strategy. (b) With FW strategy.

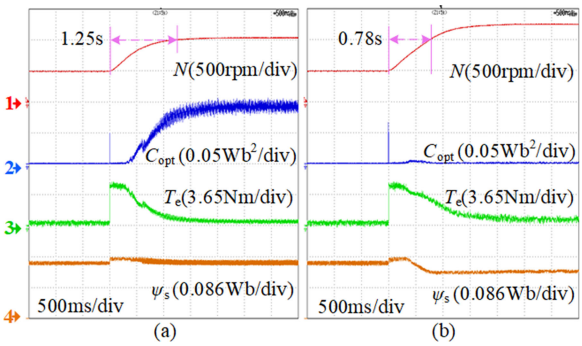

Fig. 9. Dynamic response when the reference speed changes from 500 to 1250 r/min without load. (a) Without FW strategy. (b) With FW strategy.

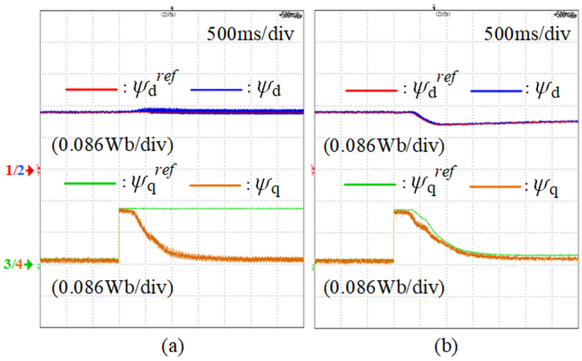

Fig. 10. Stator flux response when the reference speed changes from 500 to 1250 r/min without load. (a) Without FW strategy. (b) With FW strategy.

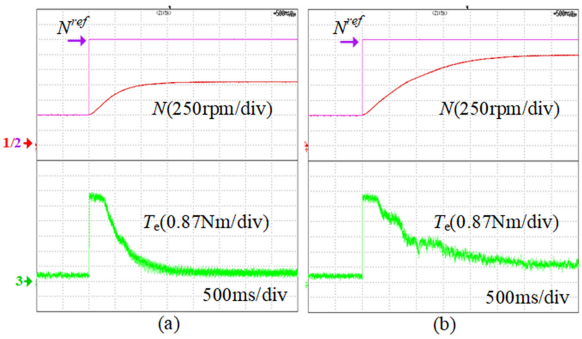

Fig. 11. Comparison of operation range and torque output of the proposed MPFC. (a) Without FW strategy. (b) With FW strategy.

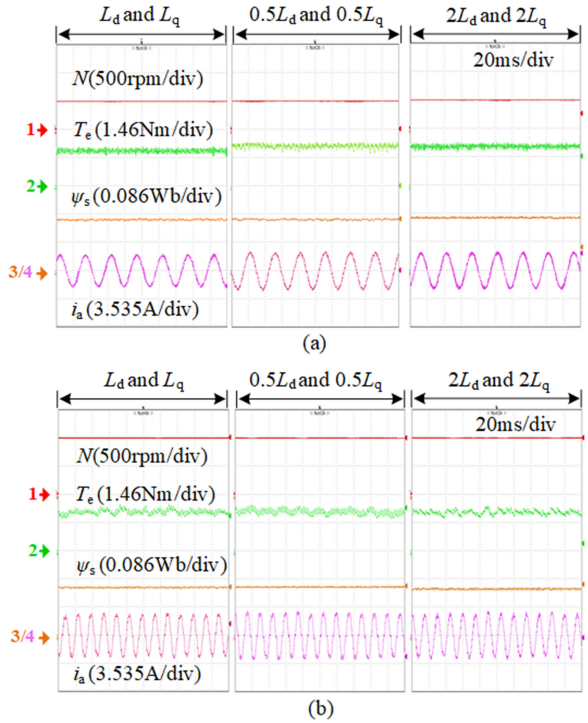

Fig. 12. Steady-state performance of the proposed strategy with different settings of L_d and L_q (a) at 500 r/min (b) at 1000 r/min.

A. Steady-State Performance

Fig. 7 shows the steady-state performance of the proposed MPFC strategy in constant torque region at 500 r/min with maximum torque output. The waveforms in Fig. 7 are speed N, electromagnetic torque T_e, amplitude of stator flux ψ_s, and stator current of phase A i_a from top to bottom. It can be seen that the PMSM operates in stable condition with low torque and flux ripples. The stator current is sinusoidal with less harmonic components. The maximum torque output of the proposed strategy at 500 r/min is 6.25 N·m and the amplitude of the stator flux is 0.172 Wb.

Fig. 8 shows the steady-state performance of the proposed method in FW region at 1000 r/min with maximum torque output. The experimental results with and without the proposed

FW strategy is compared in Fig. 8(a) and (b) when the PMSM operates with maximum achievable torque output at 1000 r/min. The waveforms in Fig. 8 are speed N, electromagnetic torque T_e, amplitude of stator flux ψ_s, and stator current of phase A i_a from top to bottom.

The maximum achievable electromagnetic torque output in Fig. 8(a) is 0.82 N·m and it is increased to 3.35 N·m with the proposed FW strategy in Fig. 8(b). With the given PMSM parameters in this paper, the theoretical optimal toque output at 1000 r/min is calculated as 3.80 N·m [22], and the experimental result is 88.8% of the theoretical value. The stator current in Fig. 8(b) is more sinusoidal with less harmonic components than that in Fig. 8(a). It can be seen from Fig. 8 that the proposed FW strategy has enhanced the steady-state performance and the maximum torque output of the PMSM in the FW region.

B. Dynamic Performance

The dynamic performances of the proposed MPFC with and without FW strategy are compared in Fig. 9 with the operation condition that the reference speed changes from 500 to 1250 r/min without load. The waveforms in Fig. 9 are speed *N*, the optimal value of cost function $C_{\rm opt}$, electromagnetic torque T_e, and amplitude of stator flux $\psi_{\rm s}$ from top to bottom. It can be seen from Fig. 9(a) that when the PMSM system enters the FW region, the optimal value of cost function $C_{\rm opt}$ increases rapidly and the output of the inverter reaches the limits. The maximum speed in Fig. 9(a) is 1025 r/min, which is lower than the reference value. With the proposed FW strategy, it can be seen from Fig. 9(b) that the optimal value of cost function $C_{\rm opt}$ is controlled to be small and the actual speed reaches the reference value. The amplitude of the stator flux decreases in the FW region, which shows the effectiveness of the FW strategy. The torque output in the FW region is also enhanced with the proposed FW strategy. It takes 1.25 s for the PMSM system without FW strategy to reach 1000 rpm in Fig. 9(a) and only 0.78 second for the PMSM system with FW strategy. It can be seen from Fig. 9 that the proposed FW strategy can realize FW operation of the PMSM system by controlling the value of the cost function. The dynamic response and output performance of the PMSM system are enhanced with the proposed FW strategy.

The stator flux responses of the PMSM system with and without FW strategy are analyzed to validate the effectiveness of the proposed FW strategy. The operation conditions are the same as that in Fig. 9. The reference value and observed value of the *d–q* components of the stator flux are shown in Fig. 10. It can be seen from Fig. 10(a) that when the PMSM operates without FW strategy, $\psi_d^{\rm ref}$ and $\psi_q^{\rm ref}$ are constant in the FW region. However, ψ_q is not able to follow the reference value $\psi_q^{\rm ref}$, which has significant influence on the torque output of the PMSM system. By applying the proposed FW strategy, ψ_d and ψ_q are able to follow $\psi_d^{\rm ref}$ and $\psi_q^{\rm ref}$, which are compensated in the FW region, as shown in Fig. 10(b).

C. Operation Range

The operation range and torque output of the PMSM system with and without FW strategy are compared in Fig. 11 with the reference speed changes from 500 to 1750 r/min without load. It can be seen from Fig. 11(a) that the maximum speed of the proposed MPFC without FW strategy is 1025 r/min. In Fig. 11(b), the maximum speed is extended to 1500 r/min with the proposed FW strategy. The operation range of the PMSM system with the FW strategy is 146% of that without the FW strategy. It can be seen from Fig. 11 that the torque output in the FW region is also enhanced with the proposed FW strategy.

D. Parameter Sensitivity

In order to analyze the parameter sensitivity of the proposed method, the control performances of the proposed method are compared when the PMSM parameters are set in different value. In Fig. 12, the steady-state performances of the proposed method with 2 N·m load in constant torque region (500 r/min) and FW region (1000 r/min) are given with different settings of L_d and L_q for comparison.

In Fig. 12(a) and (b), the values of L_d and L_q are set as the actual value (L_d and L_q), half of the actual value ($0.5L_d$ and $0.5L_q$), and twice of the actual value ($2L_d$ and $2L_q$). It can be seen from the experimental results that the control performances are nearly the same in Fig. 12(a) or (b), which indicates that the robustness of the proposed control strategy against parameter variation is pretty good in both constant torque region and FW region.

VI. Conclusion

In this paper, a modified MPFC with cost function-based FW strategy was proposed. The main contributions of this paper can be concluded as follows.

1) The prediction model and cost function of MPFC have been reconfigured using the flux increment as the control variable. A novel space flux vector plane has been proposed to explain the principle of the proposed MPFC.
2) The voltage and current limitations have been transformed as the limitation of the stator flux vector. The operation trajectories of the stator flux vector in both constant torque and FW regions have been analyzed to reveal the control objectives in different operation regions.
3) A cost function-based FW strategy has been proposed to expand the operation range of the PMSM system. The value of the cost function has been used as the FW control variable without increasing additional FW control constraints in the cost function.

References

[1] J. A. Güemes, A. M. Iraolagoitia, J. I. Del Hoyo, and P. Fernández, "Torque analysis in permanent-magnet synchronous motors: A comparative study," *IEEE Trans. Energy Convers.*, vol. 26, no. 1, pp. 55–63, Mar. 2011.

[2] R. D. Lorenz and D. B. Lawson, "Flux and torque decoupling control for field-weakened operation of field-oriented induction machines," *IEEE Trans. Ind. Appl.*, vol. 26, no. 2, pp. 290–295, Mar./Apr. 1990.

[3] A. D. Alexandrou, N. K. Adamopoulos, and A. G. Kladas, "Development of a constant switching frequency deadbeat predictive control technique for field-oriented synchronous permanent-magnet motor drive," *IEEE Trans. Ind. Electron.*, vol. 63, no. 8, pp. 5167–5175, Aug. 2016.

[4] I. Takahashi and T. Noguchi, "A new quick-response and high-efficiency control strategy of an induction motor," *IEEE Trans. Ind. Appl.*, vol. IA-22, no. 5, pp. 820–827, Sep. 1986.

[5] G. S. Buja and M. P. Kazmierkowski, "Direct torque control of PWM inverter-fed AC motors – A survey," *IEEE Trans. Ind. Electron.*, vol. 51, no. 4, pp. 744–757, Aug. 2004.

[6] F. Mwasilu, H. T. Nguyen, H. H. Choi, and J. Jung, "Finite set model predictive control of interior PM synchronous motor drives with an external disturbance rejection technique," *IEEE/ASME Trans. Mechatronics*, vol. 22, no. 2, pp. 762–773, Apr. 2017.

[7] A. Mora, Á. Orellana, J. Juliet, and R. Cárdenas, "Model predictive torque control for torque ripple compensation in variable-speed PMSMs," *IEEE Trans. Ind. Electron.*, vol. 63, no. 7, pp. 4584–4592, Jul. 2016.

[8] X. Zhang and B. Hou, "Double vectors model predictive torque control without weighting factor based on voltage tracking error," *IEEE Trans. Power Electron.*, vol. 33, no. 3, pp. 2368–2380, Mar. 2018.

[9] W. Xie *et al.*, "Finite-control-set model predictive torque control with a deadbeat solution for PMSM drives," *IEEE Trans. Ind. Electron.*, vol. 62, no. 9, pp. 5402–5410, Sep. 2015.

[10] Y. Zhang, H. Yang, and B. Xia, "Model-predictive control of induction motor drives: Torque control versus flux control," *IEEE Trans. Ind. Appl.*, vol. 52, no. 5, pp. 4050–4060, Sep./Oct. 2016.

[11] Y. Zhang and H. Yang, "Model-predictive flux control of induction motor drives with switching instant optimization," *IEEE Trans. Energy Convers.*, vol. 30, no. 3, pp. 1113–1122, Sep. 2015.
[12] C. Sun, D. Sun, Z. Zheng, and H. Nian, "Simplified model predictive control for dual inverter-fed open-winding permanent magnet synchronous motor," *IEEE Trans. Energy Convers.*, vol. 33, no. 4, pp. 1846–1854, Dec. 2018.
[13] M. Habibullah, D. D. Lu, D. Xiao, J. E. Fletcher, and M. F. Rahman, "Predictive torque control of induction motor sensorless drive fed by a 3L-NPC inverter," *IEEE Trans. Ind. Informat.*, vol. 13, no. 1, pp. 60–70, Feb. 2017.
[14] J. Liu, C. Gong, Z. Han, and H. Yu, "IPMSM model predictive control in flux-weakening operation using an improved algorithm," *IEEE Trans. Ind. Electron.*, vol. 65, no. 12, pp. 9378–9387, Dec. 2018.
[15] J. Su, R. Gao, and I. Husain, "Model predictive control based field-weakening strategy for traction EV used induction motor," *IEEE Trans. Ind. Appl.*, vol. 54, no. 3, pp. 2295–2305, May/Jun. 2018.
[16] Y. Zhang, Y. Bai, H. Yang, and B. Zhang, "Low switching frequency model predictive control of three-level inverter-fed IM drives with speed-sensorless and field-weakening operations," *IEEE Trans. Ind. Electron.*, vol. 66, no. 6, pp. 4262–4272, Jun. 2019.
[17] Z. Mynar, L. Vesely and P. Vaclavek, "PMSM model predictive control with field-weakening implementation," *IEEE Trans. Ind. Electron.*, vol. 63, no. 8, pp. 5156–5166, Aug. 2016.
[18] P. Cortes, J. Rodriguez, C. Silva, and A. Flores, "Delay compensation in model predictive current control of a three-phase inverter," *IEEE Trans. Ind. Electron.*, vol. 59, no. 2, pp. 1323–1325, Feb. 2012.
[19] Y. Cho, K. Lee, J. Song, and Y. I. Lee, "Torque-ripple minimization and fast dynamic scheme for torque predictive control of permanent-magnet synchronous motors," *IEEE Trans. Power Electron.*, vol. 30, no. 4, pp. 2182–2190, Apr. 2015.
[20] M. Preindl and S. Bolognani, Model predictive direct torque control with finite control set for PMSM drive systems, part 1 maximum torque per ampere operation, *IEEE Trans. Ind. Informat.*, vol. 9, no. 4, pp. 1912–1921, Nov. 2013.
[21] R. P. Aguilera and D. E. Quevedo, "Predictive control of power converters: Designs with guaranteed performance," *IEEE Trans. Ind. Informat.*, vol. 11, no. 1, pp. 53–63, Feb. 2015.
[22] J. SalomÄki, M. Hinkkanen, and J. Luomi, "Influence of inverter output filter on maximum torque and speed of PMSM drives," *IEEE Trans. Ind. Appl.*, vol. 44, no. 1, pp. 153–160, Jan./Feb. 2008.

Zhihao Zheng was born in 1993. He received the B.S. degree in electrical engineering in 2015 from Zhejiang University, Hangzhou, China, where he is currently working toward the Ph.D. degree.

His current research interests include power electronics and advanced control strategy of electric machine.

Dan Sun (M'05–SM'17) received the B.S. degree from Shenyang Jianzhu University, Shenyang, China, in 1997, the M.S. degree from Hohai University, Nanjing, China, in 2000, and the Ph.D. degree from Zhejiang University, Hangzhou, China, in 2004, all in electrical engineering.

In 2004, she joined the College of Electrical Engineering, Zhejiang University. Since 2017, she has been a Full Professor with Zhejiang University. Her research interests include the advanced electric machine drives and control for wind power generation system.